

# Optimization of the Correlation Range Receiver Parameters in SLR2000

John J. Degnan  
Code 920.3, Geoscience Technology Office  
NASA Goddard Space Flight Center  
Greenbelt, MD 20771 USA

## 1. INTRODUCTION

Virtually all Satellite Laser Ranging (SLR) stations produce a real-time display known as an Observed-Minus-Calculated (OMC) plot. In such a plot, illustrated in Figure 1, the horizontal axis displays the elapsed time during the track while the vertical axis displays the measured ranges to the target plus any false alarms as points on the plot. The vertical axis is dynamically centered on the predicted round trip time to the target while the vertical width of the display corresponds to the range gate width,  $\tau_g$ , which is chosen to reflect the a priori uncertainty in the range to the target. If we could predict the satellite orbits perfectly, the signal data would appear on our OMC plot as a narrow horizontal band in the center of a very narrow range gate. The width of the band,  $\delta$ , would represent the overall timing precision of our instrument (including target effects) which, for modern SLR systems would have a total width between  $3\sigma$  points on the order of 0.5 nsec or less for geodetic satellites. In reality, there is always a range bias (which moves the data vertically within that gate) and a time bias which, when multiplied by the range acceleration, introduces a slope  $\sigma$  in the OMC data display.

The principal difference in the OMC plots of a conventional high SNR system and a photon-counting system (especially in daylight) is the presence of a large background of single photon false alarms, which are produced by a variety of noise sources to be discussed in later sections. The density of signal points also increases, especially at higher elevation angles, due to the orders of magnitude increase in laser repetition rate from 5 or 10 Hz to 2000 Hz in SLR2000.

The extraction of single photon satellite returns from the solar background during daylight tracking relies on the "temporal coherence" of the signal returns, as exemplified by the narrow band of data in Figure 1, and is accomplished in SLR2000 by a "Correlation Range Receiver" (CRR) [Degnan, 2001]. In a CRR, the range gate is divided into a number of equally sized *range bins* of duration  $\tau_b$ , and the photon counts in each bin are summed over a sampling period  $\tau_f$  called the *frame interval*. In Figure 1, the horizontal lines representing the range bin borders and the vertical lines representing the boundaries between frames enclose a 2D area, which we refer to as a *cell*. Cells containing signal counts are *signal cells* whereas cells containing only noise are *noise cells*.

In a CRR, the photon counts in each cell, resulting from the cumulative effect of single photon satellite laser returns and background noise counts, are compared to a *frame threshold*. If the count exceeds the threshold, the bin is tentatively judged to contain signal whereas, if the count falls below the threshold, that particular bin is deemed to contain only noise. The optimum choice of range bin size, frame interval, and threshold will not only vary from satellite to satellite but will also depend on the instantaneous performance of the laser and receiver as well as local meteorological conditions, both of which can affect the mean received signal counts and the solar noise background. Thus, the correlation receiver design must be flexible enough to adapt to changing operating and meteorological conditions and targets. It must also be able to deal with occasional data dropouts as might be caused by intervening clouds, telescope pointing errors, etc. The manner in which the cell dimensions are optimally chosen will be discussed later.

## OMC PLOT AND CORRELATION RANGE RECEIVER

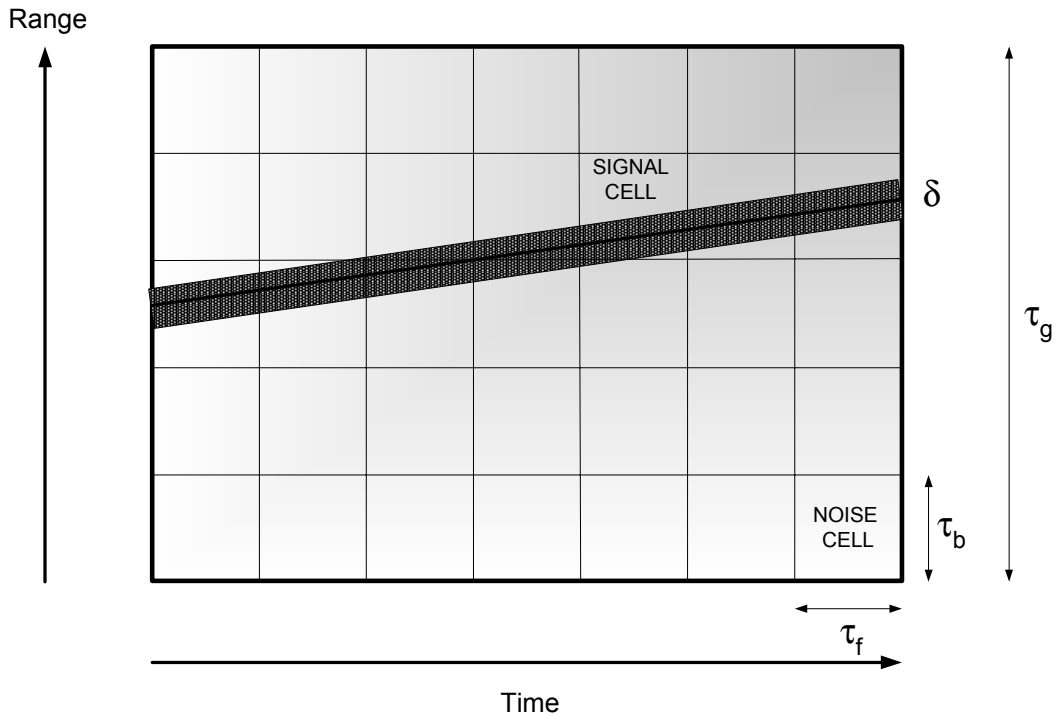


**Figure 1: The real-time OMC display of a photon-counting satellite laser ranging system will show a sloped narrow band of temporally coherent signal data against a background of noise counts. In a Correlation Range Receiver (CRR), the range gate,  $\tau_g$ , is divided into equal range bins of duration,  $\tau_b$ , and the time axis is broken into units,  $\tau_f$ , called the frame interval. The resulting 2-D elements are called “cells”, and the total counts in each cell are compared to a “frame threshold” to determine if they contain signal or just noise.**

In order to maintain maximum flexibility and fully optimize the parameters of such a receiver over a wide dynamic range of both signal and noise, the system must be controlled in real time by software that can combine a priori information on the satellite link with real time sensor data. The goal, of course, is to achieve a high probability of signal detection combined with excellent noise rejection that is largely independent of local atmospheric conditions. Default values for bin size, frame interval and threshold are computed and stored in the software based on a nominal ranging link, an a priori solar noise model, and the maximum expected range and time biases in the orbit prediction for a given satellite. During ranging operations, the measured count rates can be compared to the computed a priori values in real time and the receiver parameters adjusted as necessary via algorithms to be described in this paper.

The algorithms are based on the maximization of the "Differential Cell Count" (DCC), which is the difference between the number of cells per frame correctly identified as signal minus the number of false alarm cells [Degnan, 2002a]. The DCC has an ideal value of one, corresponding to 100% probability of detection and zero false alarms per frame. The present paper reviews the methodology by which the default receiver settings can be optimized and the manner in which they can be updated rapidly in the presence of sensor readings that deviate from their expected

values. Numerical results for LAGEOS will be presented throughout the paper assuming a standard clear atmosphere (horizontal visibility = 23 km). The SLR2000 system parameters to be used in the analyses are summarized in Table 1

Wavelength, $\lambda$	532 nm
LAGEOS Cross-section, $\sigma_t$	$7 \times 10^6 \text{ m}^2$
Laser Fire Rate, $f_{os}$	2 kHz
Transmitted Laser Energy, $E_t$	133 $\mu\text{J}$ (eyesafe at exit aperture)
Average Transmitted Laser Power, $P_t$	266 mW (at exit aperture)
Height of station above sea level, $h_s$	0 m (worst case)
One-way Atmospheric Transmission at Zenith, $T_0$	0.7 (Standard Clear, 23 km visibility)
Exo-atmospheric solar irradiance, $N_\lambda$	$0.2 \text{ W/m}^2\text{-ster-A}^\circ$
Exo-atmospheric lunar Irradiance (Full Moon)	$4.8 \times 10^{-7} \text{ W/m}^2\text{-ster-A}^\circ$
FWHM Bandwidth, spectral filter, $\Delta\lambda$	$3 \text{ \AA}^\circ$
Transmitter Divergence Half-Angle, $\theta_t$	25 $\mu\text{rad}$
RMS Transmitter Pointing Error, $\sigma_p$	15 $\mu\text{rad}$
Receiver FOV Half Angle, $\theta_r$	50 $\mu\text{rad}$
Telescope Primary Diameter, $D_r$	40 cm
Atmospheric Scale Height, $h_{sc}$	1.2 km
Detector Quantum Efficiency, $\eta_q$	0.13 (Photek Quadrant MCP/PMT)
Detector Dark Count	50 kHz (Photek Quadrant MCP/PMT)
Receiver Throughput Efficiency, $\eta_r$	0.40
Range Gate, $\tau_g$	200 nsec (McGarry et al)
Maximum Orbital Time Bias, $t_{bias}$	2 msec (McGarry et al)
Maximum Range Acceleration, $R_{acc}$	10 nsec/sec <sup>2</sup> (McGarry et al)
Maximum Data Slope, $\sigma$	0.02 nsec/sec
Range Bin, $\tau_b$	2 nsec
Data Spread, $\delta$	0.4 nsec ( $\pm 3\sigma$ )

**Table 1: Parameters used in LAGEOS 1 Link Analyses**

## 2. MEAN SIGNAL COUNT PER CELL

The mean number of photoelectrons detected per laser fire is given by the link equation [Degnan, 1993]

$$\langle n_s \rangle = \frac{4\eta_q \sigma_t \eta_r T_0^{2 \sec \theta_r}}{h\nu \theta_t^2 (4\pi)^2} \frac{E_t A_r}{R^4} \frac{1}{1 + \left( \frac{\sigma_p}{\theta_t} \right)^2} \quad (1)$$

which depends on the transmitter energy  $E_t$ , the effective area of the receive telescope  $A_r$ , the target range  $R$ , the detector quantum efficiency  $\eta_q$ , the photon energy  $h\nu$ , the one-way atmospheric transmission at zenith  $T_0$ , the local zenith angle (complement of elevation angle) of the target satellite  $\theta_r$ , the divergence half-angle of the laser beam  $\theta_t$ , the target optical cross-section  $\sigma_t$ , the RMS pointing error  $\sigma_p$ , and the throughput efficiencies of the transmitter ( $\eta_t$ ) and receiver ( $\eta_r$ ) optics respectively. Equation (1) assumes there is a random pointing error but no net

pointing bias. For the photon-counting SLR2000 system, we typically have  $n_s \ll 1$ , and this is especially true for the higher satellites and low elevation angles. The expected mean signal count per pulse and range returns per second for LAGEOS are plotted in Figure 2.

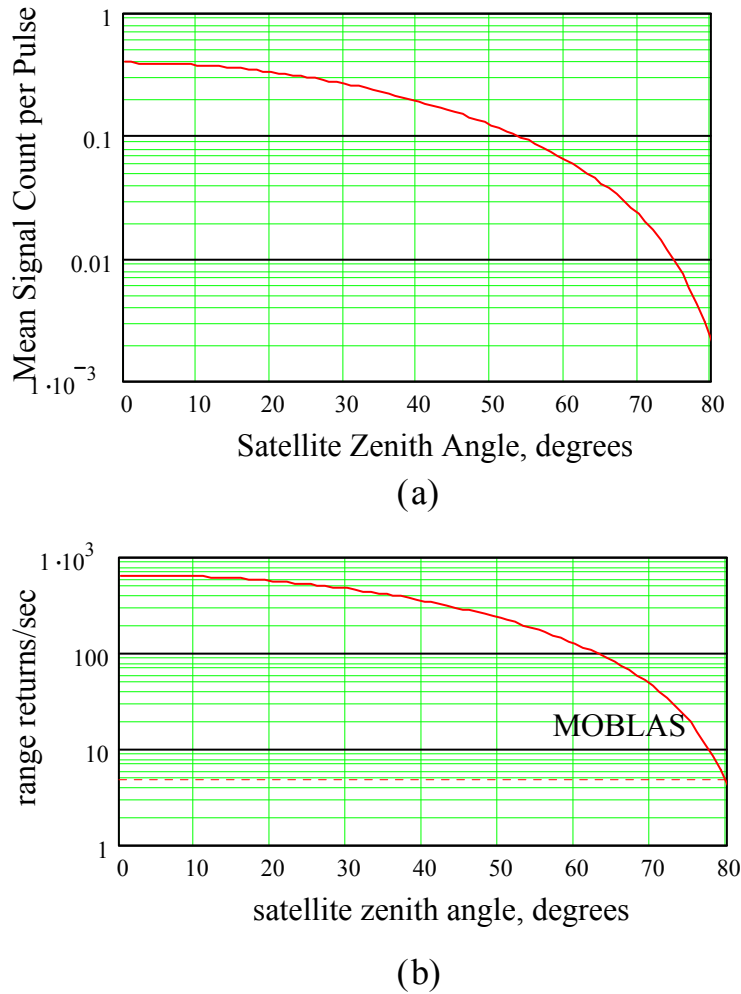


**Figure 2: Mean signal count (a) and range return rate (b) expected for LAGEOS as a function of satellite zenith angle (complement of the elevation angle) in a standard clear atmosphere. Note that the expected range return rate exceeds the maximum MOBLAS rate of 5 pps, even at low elevation angles.**

Over a frame interval, the mean number of signal photoelectrons collected in the signal cell is given by

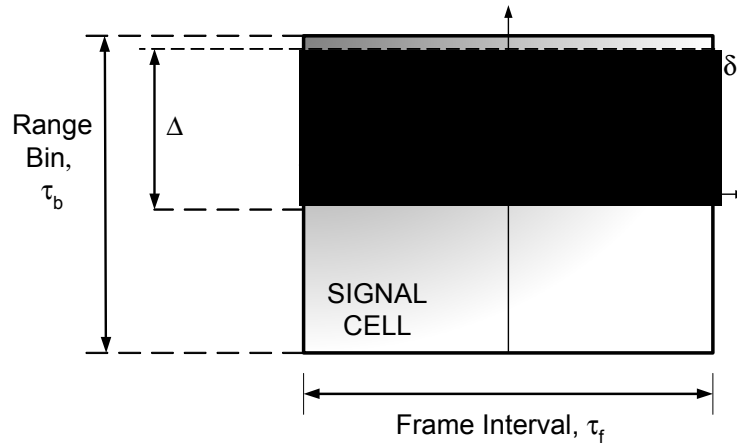
$$N_s = f_{QS} \tau_f \langle n_s \rangle \quad (2)$$

where  $f_{QS}$  is the laser fire rate and  $\tau_f$  is the frame interval defined in Figure 1. Equation (2) assumes that the range bin is chosen large enough to collect all of the signal counts in a given frame, at least most of the time. There will always be instances, however, where the signal count is shared between an adjacent vertical cell as in Figure 1. In the worst case situation, two cells

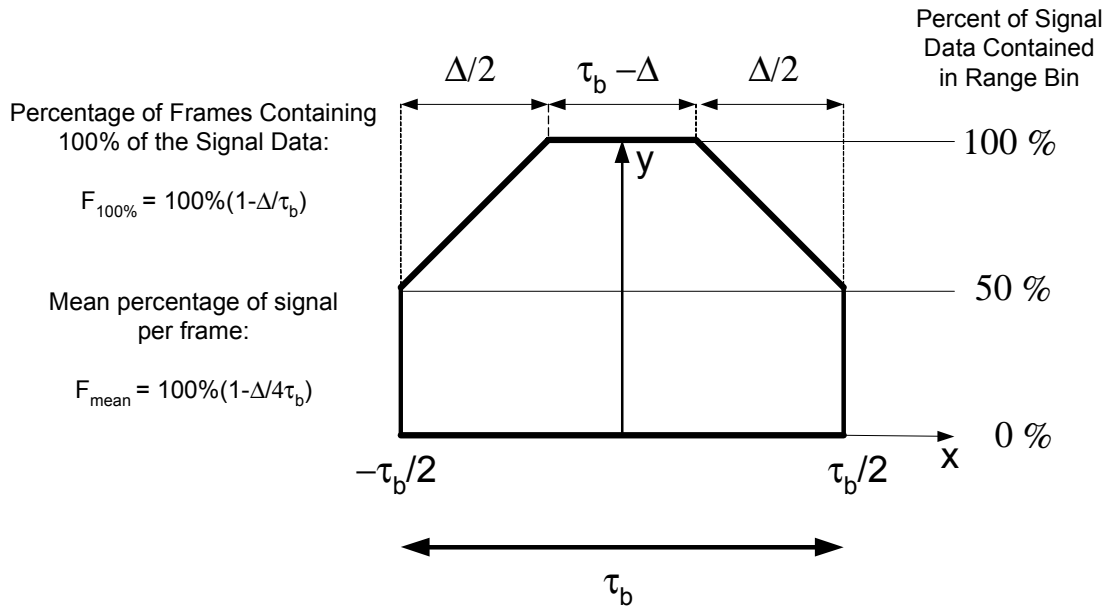
will share the signal data equally. Figure 3a provides a closeup view of a signal cell. The total fraction of the range bin interval occupied by the signal is given by

$$\Delta = \delta + |\sigma\tau_f| \quad (3)$$

where  $\delta$  is the width of the data band,  $\sigma$  is the slope of the data band, and  $\tau_f$  is the frame interval.



(a)



(b)

**Figure 3: (a) Closeup of a signal cell in which the parameters  $\delta$ ,  $\Delta$ , and  $x$  are defined; (b) Percentage of the signal returns contained in the cell as a function of the distance  $x$  of the data band center from the center of the cell.**

Figure 3b shows the percentage of signal counts contained in the signal cell as a function of the vertical distance  $x$  of the data band center from the geometric center of the cell. At values of  $x = \pm \tau_b/2$ , the signal count falls to a minimum of 50% (i.e. the data is shared equally with one of the two adjacent vertical cells), and there is a band of width  $\tau_b - \Delta$  in the center where 100% of the signal counts fall within the cell. Since the data band center has an equal probability of falling anywhere within the cell along the vertical range axis, it is easily shown from Figure 3b that the percentage of time 100% of the signal falls into a single cell is given by the equation

$$F_{100\%} = 100\% \left( 1 - \frac{\Delta}{\tau_b} \right) = 100\% \left( 1 - \frac{1}{\beta} \right) \quad (4a)$$

and the mean percentage of signal counts falling within the signal bin is given by

$$F_{mean} = 100\% \left( 1 - \frac{\Delta}{4\tau_b} \right) = 100\% \left( 1 - \frac{1}{4\beta} \right) \quad (4b)$$

respectively, where we have defined a range bin to data spread ratio

$$\beta \equiv \frac{\tau_b}{\Delta} \geq 1 \quad (4c)$$

Equations (4a) and (4b) are plotted as a function of  $\beta$  in Figure 4.

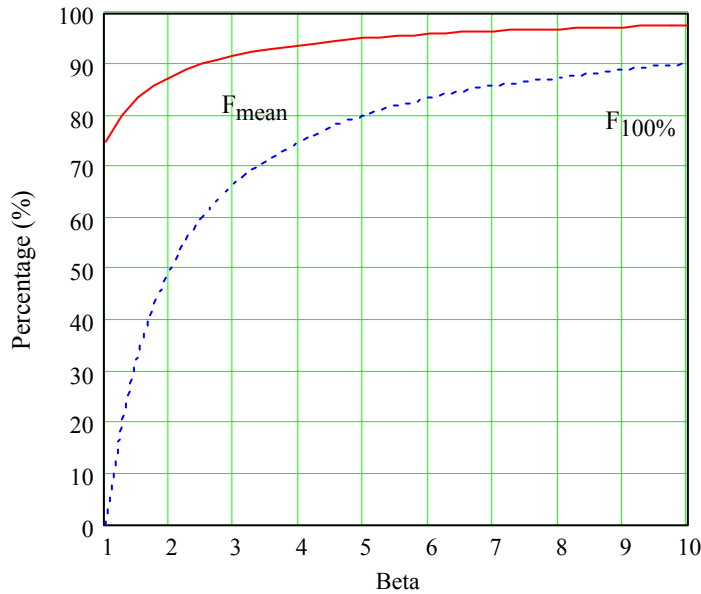


**Figure 4: Mean percentage of signal counts contained in the signal cell over many frames (solid curve) and the percentage of signal cells containing 100% of the signal data (dashed curve) as a function of the range bin to data spread ratio,  $\beta = \tau_b/\Delta$ .**

### 3. MEAN NOISE COUNT PER CELL

Sources of noise in SLR2000 include: (1) detector dark counts (internal noise unrelated to the local light environment), (2) the stellar or near-horizon manmade light background within the receiver field of view (FOV), (3) the scattering of sunlight (or moonlight) off the local atmosphere, and (4) backscatter of the transmitted laser radiation off the instrument optics or atmosphere. The last two noise sources are dominant, and we will therefore base our assessment of SLR2000 performance under the worst case conditions of daytime solar illumination and coaxial laser backscatter. Since we have incorporated sun avoidance software in SLR2000, we will ignore those relatively rare incidences when the satellite passes directly in front of the Sun or sunlit Moon.

Direct solar (or lunar) illumination of the receiver front end optics and the resulting scatter within the instrument is another potential source of background noise. Stray light rejection is therefore an important consideration, especially when SLR2000 is operating close to the Sun or Sunlit Moon. SLR2000 is therefore equipped with a narrow spatial field of view filter, a blackened honeycomb sun shield at the entrance window to the telescope, a light-tight receiver box on the transceiver table, and Sun avoidance software.

Dark count rates in the visible detectors typically used in laser ranging tend to be relatively low (on the order of  $10^4$  counts/sec or less) compared to daytime solar background rates on the order of  $10^6$  counts/sec. The quadrant microchannel plate photomultiplier developed by Photek Ltd. for SLR2000 has a guaranteed dark count rate less than  $5 \times 10^4$  counts per second which implies an average of only 0.05 dark counts in a one microsecond range gate.

When operating under local daylight conditions, the noise background rate caused by solar scattering in the local atmosphere is given by the expression [Degnan, 2002b]

$$\begin{aligned} \dot{n}_{is} &= \frac{\eta_q \eta_r}{h\nu} \frac{N_\lambda (\Delta\lambda) A_r \Omega_r}{4\pi} \left\{ \sec \theta_T T_0^{\sec \theta_T} \left[ \frac{1 - T_0^{\sec \theta_S - \sec \theta_T}}{\sec \theta_S - \sec \theta_T} \right] \right\} \\ &\cong \frac{\eta_q \eta_r}{h\nu} \frac{N_\lambda (\Delta\lambda) A_r \Omega_r}{4\pi} \left\{ T_0^{\sec \theta_T} \ln \left( \frac{1}{T_0^{\sec \theta_T}} \right) \right\} \end{aligned} \quad (5)$$

where  $N_\lambda = 0.2 \text{ W/m}^2\text{-ster-A}^\circ$  is the exoatmospheric solar spectral irradiance at the operating wavelength of 532 nm,  $\Delta\lambda$  is the FWHM spectral bandwidth of the receiver, and  $\Omega_r$  is the receiver field of view in steradians. It should be mentioned that the atmospheric noise model makes no assumptions regarding the distribution of scatterers with altitude. The model makes the common assumption of no horizontal gradients, however, and therefore depends only on the one-way zenith transmission,  $T_0$ , between the station and the "top" of the planetary atmosphere and the local zenith angles of the Sun,  $\theta_S$ , and of the target,  $\theta_T$ . Note that as  $T_0 \rightarrow 1$  (no scattering atmosphere), the background count rate due to solar scatter off the atmosphere correctly goes to zero, due to the logarithmic term, for all values of  $\theta_S$  and  $\theta_T$ . The second expression in (5) is an approximation which is independent of the solar angle,  $\theta_S$ . Although the approximation is strictly valid when  $\theta_S \sim \theta_T$  or when  $T_0$  is close to unity, it also gives good results for  $\theta_T < 60^\circ$  for nominally clear atmospheres ( $T_0 \geq 0.7$ ) and all values of  $\theta_S$  [Degnan, 2002b].

During night operations, the irradiance of the local atmosphere by the Moon produces background rates that are approximately six orders of magnitude lower than peak daytime values .

For example, a Full Moon produces an exoatmospheric spectral irradiance of  $4.8 \times 10^{-7} \text{ W/m}^2\text{-ster- A}^\circ$  at 532 nm. This value can be substituted into (5) to simulate atmospheric scattering backgrounds under “Full Moon” conditions.

Back-scattered laser radiation produced by the outgoing pulse is an additional time-dependent source of noise and is nominally the same for day and night operations. The use of separate transmit/receive paths (i.e. a *bistatic* configuration) is often used to suppress laser backscatter effects, but this was not an option for SLR2000 since the outgoing transmitter must fill the common 40 cm telescope aperture in order to meet OSHA eye safety standards at the exit pupil of the system. In order to contend with the high level of backscatter in the immediate vicinity of the telescope, the SLR2000 receiver is gated off for a short period following pulse emission when the backscatter is most intense. Occasionally, as the satellite range varies during the pass, a signal photon from the satellite will arrive during this “blinking” period. Instead of accepting this periodic loss of signal, SLR2000 predicts its occurrence and varies the laser pulse repetition rate slightly so the returning photons never arrive during the receiver “blinking” period.

For a monostatic system (coaxial transmitter and receiver optics) such as SLR2000, the backscatter contribution is given by the lidar equation [Degnan, 2002b]

$$\dot{n}_{bs}(\tau) = \frac{\eta_q \eta_r A_r}{2\pi h \nu} \frac{E_t}{h_{sc} c} \left[ \ln \left( \frac{1}{T_0} \right) T_0^{2 \sec \theta_T} \left[ 1 - \exp \left( -\frac{c\tau}{2h_{sc} \sec \theta_T} \right) \right] \right] \left[ \frac{\exp \left( -\frac{c\tau}{2h_{sc} \sec \theta_T} \right)}{\tau^2} \right] \quad (6)$$

and falls off rapidly with the time from laser fire defined by

$$\tau = \frac{2s}{c} = \frac{2 \sec \theta_T}{c} (z - h_s), \quad (7)$$

where  $s$  is the distance from the terminal to the scattering volume,  $h_s$  is the altitude of the station above sea level,  $z$  is the altitude of the scattering volume, and  $h_{sc}$  is the atmospheric scale height. Due to the logarithmic term in (6), the backscatter contribution correctly goes to zero in the absence of a scattering atmosphere.

We can now compute the mean number of noise counts collected in any given cell (including the signal cell) by summing over the various sources of noise

$$N_b(\tau) = f_{QS} \tau_f \tau_b \left[ \dot{n}_{ls} + \dot{n}_{bs}(\tau) + \dot{n}_d \right] \quad (8)$$

where  $\dot{n}_d$  is the dark count rate. The *signal cell contrast* is defined as the total mean number of counts in the signal cell (including noise) divided by the mean noise count. Using (2), (4b) and (8), we obtain for the contrast

$$C(\tau) = \frac{N_s + N_b(\tau)}{N_b(\tau)} = 1 + \frac{\langle n_s \rangle F_{mean}}{\tau_b \left[ \dot{n}_{ls} + \dot{n}_{bs}(\tau) + \dot{n}_d \right]} = 1 + \frac{\langle n_s \rangle}{\Delta \left[ \dot{n}_{ls} + \dot{n}_{bs}(\tau) + \dot{n}_d \right]} \left[ \frac{1}{\beta} \left( 1 - \frac{1}{4\beta} \right) \right] \quad (9)$$

where we have included the effects of truncation of the data by the range bin boundaries. We note from (9) that the signal contrast does not change with the choice of frame interval except to the extent that it influences the value of  $\Delta$  via (3). Choosing too large a range bin (proportional to  $\beta$ ), however, can reduce the contrast significantly. A value  $\beta = 1$  maximizes the contrast but, on average, only picks up 75% of the data in the signal cell. Values of  $\beta$  between 2 and 4 represent a good compromise between capturing a large fraction (87% to 94%) of the signal returns in a single cell per frame while maintaining a high signal contrast. Once the data slope is detected and removed by the system computer by applying an updated time bias,  $\Delta$  collapses to the smaller instrumental data width,  $\delta$ , and the signal cell will collect a still higher percentage of the signal counts on average via (4b).

In Figure 5a, we plot the contrast for LAGEOS as a function of the satellite zenith angles for solar angles of 0 (high noon), 20, 40, 60, and 80 (dusk) degrees. At night, the contrast in Figure 5b is typically an order of magnitude higher and, since the different zenith angle of the Full Moon collapse into a single curve, is clearly dominated by the detector dark count rate.

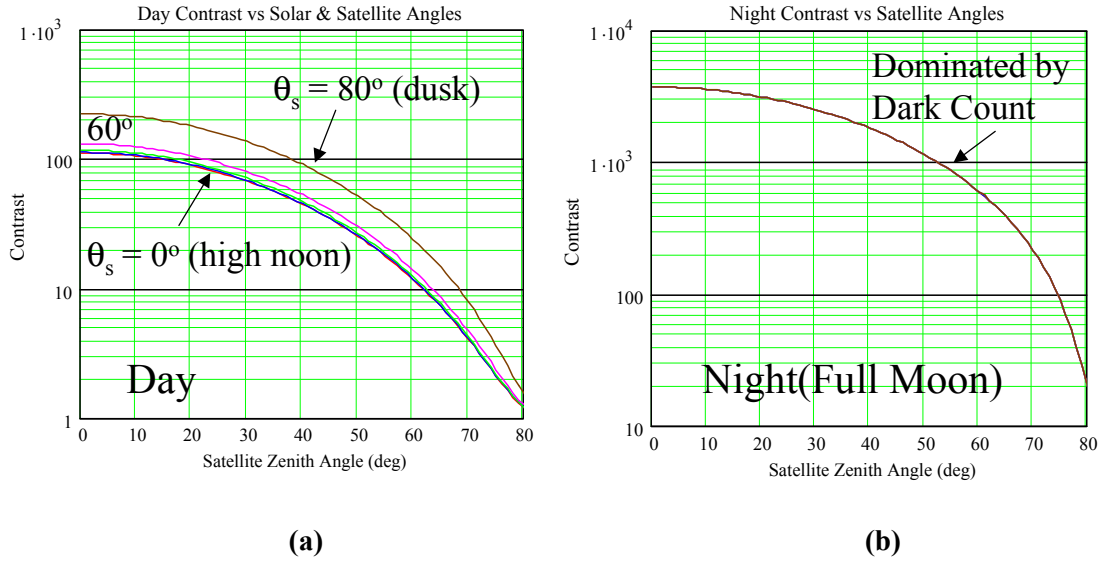


**Figure 5: Computed signal cell contrast as a function of satellite zenith angle and (a) the solar zenith angle – 0° (bottom curve or “high noon”), 20°, 40°, 60°, and 80° (top curve or “dusk”) - during daylight operations and (b) the lunar zenith angle of a Full Moon at night. In (b) the curves overlap because the photodetector dark counts far exceed the effect of moonlight scattered in the atmosphere. These results assume a 2 nsec range bin, a standard clear atmosphere, and no overlap of the return signal with the laser backscatter off the atmosphere.**

Laser backscatter significantly reduces the contrast relative to the values plotted in Figure 6 for some time period following the laser fire. This is illustrated in Figures 6a (day) and 6b (night) as a function of the time after fire for several satellite zenith angles (0, 20, 40, 60, and 80 degrees). Although the effect lasts longer at large satellite zenith angles due to longer slant ranges through the atmosphere, solar scattering rapidly becomes the dominant noise mechanism during day operations between 60 to 80 microseconds after laser fire. At night, laser backscatter degrades the contrast for up to 200 microseconds at large zenith angles before being dominated by the detector dark count rate. Except for the lowest elevation angles, contrasts typically exceed 2 beyond about 25 to 30  $\mu\text{sec}$  following the laser fire. Since the fire interval between pulses is 500  $\mu\text{sec}$ , about 5 to 6 % of the signal will be lost during the blackout period unless, as stated previously, one varies the laser fire rate slightly to avoid the temporal overlap of the outgoing pulse with the incoming signal.

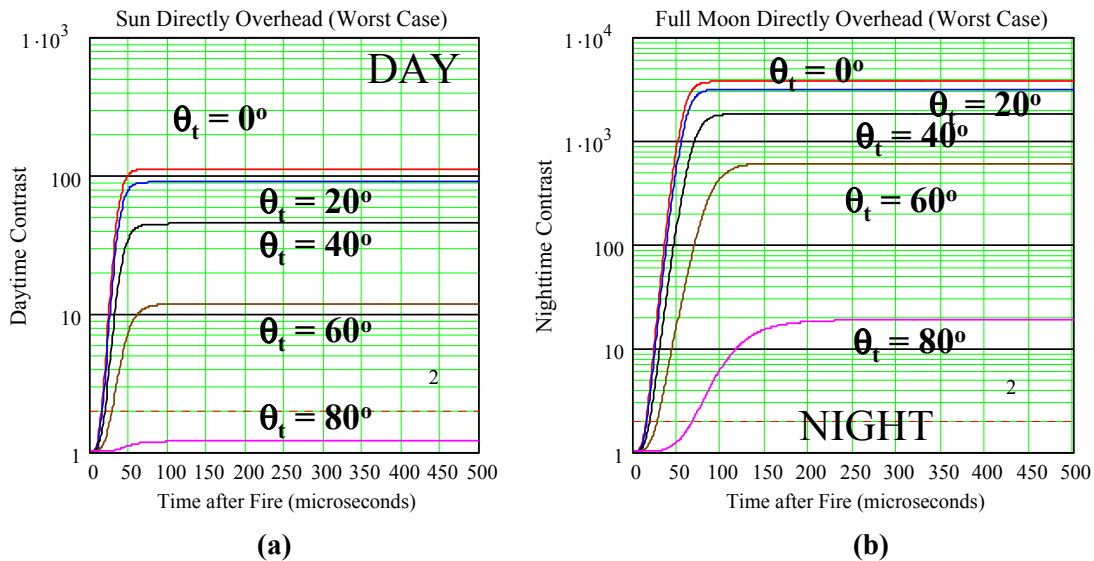


**Figure 6: Effects of laser backscatter off the atmosphere on signal contrast during day (a) and night (b) operations as a function of time after laser fire and several satellite zenith angles (0, 20, 40, 60, and 80 degrees).**

#### 4. DIFFERENTIAL CELL COUNT ALGORITHM

The *frame detection threshold*,  $K$ , is used to determine the probable presence of signal against a noise background. For single pulse detection in a conventional high SNR system, the threshold is usually set by hardware to a few photoelectrons per pulse to minimize false alarms generated by background noise. This type of noise reduction has been referred to as “amplitude filtering” [Degnan, 1985] and is used in high SNR systems along with other types of noise and false alarm reduction techniques such as spectral (narrowband filters), spatial (field stop apertures), and temporal (range gating) filters. In SLR2000, the hardware threshold is set low enough to allow detection of single photons, and “amplitude filtering” can only be applied by accumulating counts from a series of laser fires in the cells of our CRR and then comparing the counts in each cell to a frame threshold. The CRR accepts cells with mean counts above the frame threshold as containing signal and tentatively rejects cells with counts below the threshold as noise [Degnan, 2002a]. In short, high SNR systems set their thresholds based on a single laser fire whereas photon-counting systems require that we combine multiple pulses to distinguish signal from noise.

In either case, choosing too high a threshold results in the loss of valid range returns, whereas choosing too low a threshold results in an increased number of noise-induced false alarms. Furthermore, because of the potentially large number of cells in a frame (especially during acquisition when range uncertainties and gate widths are largest), it is possible that a sizable number of noise cells in a given frame will be falsely identified as signal even when the probability of false alarm for any given noise cell is relatively small. One highly effective approach to optimizing the frame threshold is to maximize the *Differential Cell Count (DCC)*, defined as the mean number of correctly identified signal cells minus the mean number of noise cells registering as false alarms within a particular frame, i.e.

$$\delta N = P_d - N_{bin} P_{fa} \quad (10)$$

where  $P_d$  is the Poisson probability of correctly identifying the signal cell within a frame,  $P_{fa}$  is the Poisson probability of falsely identifying any given noise cell as signal, and  $N_{bin}$  is the number of range bins in the range gate (or equivalently cells in a frame). The cell detection threshold that maximizes the DCC is given by [Degnan, 2002a]

$$K_{opt} = \frac{N_s + \ln N_{bin}}{\ln C} = \frac{(C-1)N_b + \ln N_{bin}}{\ln C} \quad (11)$$

where  $N_s$  is the mean signal count in the signal cell,  $N_b$  is the mean noise count per cell, and  $C$  is the signal cell contrast as defined by (2), (8), and (9) respectively. From Poisson statistics, the probability of correctly detecting the signal cell is given by

$$\begin{aligned} P_d &= \exp(-CN_b) \sum_{k=K_{opt}}^{\infty} \frac{(CN_b)^k}{k!} \\ &\cong \frac{1}{\sqrt{2\pi CN_b}} \int_{K_{opt}}^{\infty} dN \exp\left[-\frac{(N-CN_b)^2}{2CN_b}\right] = \frac{1}{2} \left[ 1 + \operatorname{erf}\left(\frac{CN_b - K_{opt}}{\sqrt{2CN_b}}\right) \right] \end{aligned} \quad (12)$$

where, in the limit of "large" mean counts ( $CN_b > 15$ ), we can use the Central Limit Theorem to approximate the Poisson distribution by a Gaussian (normal) distribution. In (12),  $\operatorname{erf}(x)$  is the familiar **error function**. Similarly, the probability that any given noise cell registers a false alarm can be written as

$$P_{fa} = \exp(-N_b) \sum_{k=K_{opt}}^{\infty} \frac{(N_b)^k}{k!} \cong \frac{1}{\sqrt{2\pi N_b}} \int_{K_{opt}}^{\infty} dN \exp\left[-\frac{(N-N_b)^2}{2N_b}\right] = \frac{1}{2} \left[ 1 - \operatorname{erf}\left(\frac{K_{opt} - N_b}{\sqrt{2N_b}}\right) \right] \quad (13)$$

where again the approximation holds quite well for  $N_b > 15$ . Finally, the mean number of false alarms per frame is given by the product  $N_{bin} P_{fa}$ .

The calculations presented in Figure 5 indicate that, during daylight acquisitions at very low elevation angles of  $10^\circ$ , the expected contrast can drop to a minimum value of about  $C = 2$  where,

from (7), we note that the mean signal counts equal the mean noise counts in the cell. However, it has been shown that, even with such low signal contrasts, the probability of correctly identifying the signal cell is virtually unity if we choose a sufficiently long frame interval such that the signal cell will contain 80 or more signal photoelectrons [Degnan, 2002a]. It was also shown that, under conditions of higher contrast, even fewer signal counts were required as summarized in Table 2.

Contrast, $C$	Required Signal Counts per Frame, $N_s$
2	80
3	50
5	35
10	25

**Table 2: Combinations of contrast and mean signal counts per frame which provide excellent ability to discriminate signal from noise.**

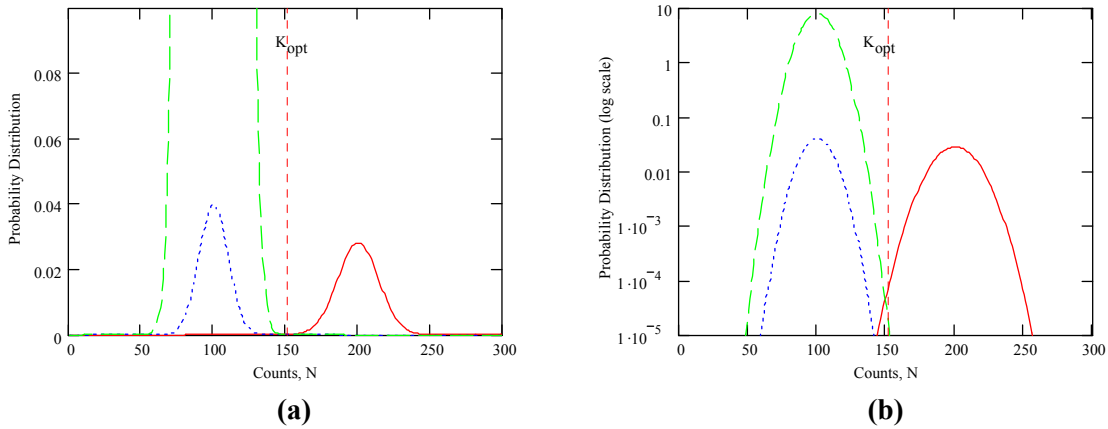


**Figure 7: Probability distributions for the count numbers in the signal cell (red solid line) and noise cell (blue dotted line) as well as the noise cell distribution multiplied by the number of range bins  $N_{bin}$  (green dashed curve) plotted on a linear scale (a) and logarithmic scale (b). The plots assume a low contrast  $C = 2$  with  $N_s = N_b = 100$ .**

The normalized probability distributions for the number of counts in the signal and noise cells are described by the Gaussian functions in (12) and (13) and illustrated in Figure 7a where we have assumed  $N_s = N_b = 100$  corresponding to a contrast  $C = 2$ . The probability distribution for the signal cell counts (solid red curve) peaks at 200 counts, due to the combination of signal plus noise counts, whereas a cell containing only noise (dotted blue curve) peaks at 100 counts. In addition, we have multiplied the noise cell by the number of range bins (green dashed curve) and plotted all of the results on a logarithmic scale in Figure 7b to capture the peak of the green dashed curve. Note that the optimum frame threshold,  $K_{opt}$ , indicated by the vertical dashed line in both graphs, lies very close to the point where the red solid and green dashed lines intersect. Integrating the solid red curve to the right of  $K_{opt}$  yields the probability of detecting the signal cell which is clearly very near unity. Integrating over the blue dotted and green dashed curves to the right of  $K_{opt}$ , gives the probability of falsely identifying a given noise cell as signal and the mean number of false alarms per frame, both of which are very near zero. Had we chosen a much shorter frame interval, the ratio of mean counts within the signal and noise cells would still be 2 to 1 but the distributions would move closer together and have significantly more overlap,

thereby forcing the optimum threshold deeper into both distributions and resulting in much poorer signal discrimination.

## 5. CONCLUSIONS

For night operations, the signal contrasts in Fig. 5b are high ( $C > 50$ ) for all LAGEOS elevation angles above  $10^\circ$  and independently of the Moon phase. We have not specifically considered the occasional bright star(s) that may pass through the receiver FOV in our analysis, but this is expected to be a relatively small and brief effect. Clearly, LAGEOS acquisition during daylight places the biggest demands on the Correlation Range Receiver. From Fig 5a, the signal contrast is degraded to values between 2 and 3 at very low elevation angles ( $10^\circ$ ). This is due not only to the reduced signal count rate resulting from an increased slant range and atmospheric losses (see Fig. 2b) but also because we are looking at the satellite through a greater volume of scattering atmosphere with a corresponding increase in solar noise background. Longer frame intervals are therefore necessary to accumulate the required number of signal photoelectrons. Figure 8a shows the frame interval required to accumulate 100 signal photoelectrons as a function of LAGEOS zenith angle in a standard clear atmosphere. It varies from a few tenths of a second over most of the pass to 2 sec at  $70^\circ$  and 20 sec at  $80^\circ$ . In Figure 8b, we compute the total data spread  $\Delta$  from (3). Except for large zenith angles near acquisition, the total spread varies only slightly from the instrumental spread  $\delta$  due to the small slope ( $\sigma = 0.02$  nsec/sec) expected for LAGEOS. The small slope results from a combination of low range acceleration during acquisition and a small time bias (see Table 1). Slopes for lower satellites are expected to be significantly higher,  $\sim 3$  nsec/sec for Starlette using data from [McGarry et al, 1996], but their range return rates and contrasts will be higher as well resulting in shorter multiplicative frame intervals in (3).

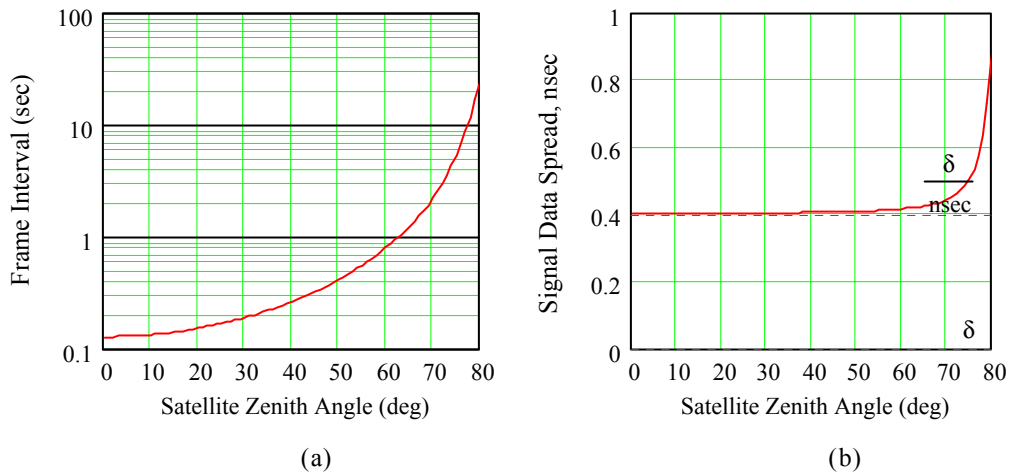


**Figure 8: (a) Frame interval required to collect 100 signal photoelectrons as a function of satellite zenith angle; (b) Corresponding data spread  $\Delta$  in nsec.**

Things improve rapidly if we acquire LAGEOS at higher elevations. At zenith angles of  $70^\circ$ , for example, a contrast of 10 or greater (see Fig 5a) allows the required counts to be reduced from 100 to 25 (from Table 2) thereby reducing the required frame interval from 2 sec to 0.5 sec. For most of the pass following acquisition, one can choose to fix the sizes of the frame interval and range bin for simplicity of operation. There is no real penalty for maintaining a larger than necessary frame interval, especially after the slope has been corrected by an updated time bias. At the higher contrasts, the practical impact of a reduced range bin is also lessened since the peaks in Fig. 7 move farther apart and signal discrimination improves at higher elevations.

Recent improvements in detector technology will further improve the speed of acquisition by reducing the frame interval. Multianode GaAsP PMT's, with quantum efficiencies of 40%, are now commercially available from Hamamatsu but are significantly more expensive (4X) than the prototype quadrant Microchannel Plate Photomultiplier (MCP/PMT) developed for SLR2000, whose conventional bi-alkali photocathode has a nominal QE of 13% at 532 nm. Thus, the higher efficiency tube can reduce the frame intervals required for acquisition by almost a factor of 4. Although PMT QE's are generally lower than that of Avalanche Photodiodes (APD's), we believe photomultipliers have several important advantages for this particular application including large active areas, low dark noise, zero dead time in photon-counting mode, ease of manufacture, and low fabrication cost.

Speed of acquisition and data rates will also depend on local meteorological conditions. Our assumption of a Standard Clear Atmosphere in the link calculations represents neither the best operating condition nor the worst. SLR2000's "smart meteorological station" makes measurements of both cloud cover and ground visibility, and SLR2000's Sun avoidance software keeps track of the Sun's position. The ground visibility data can be related to the zenith atmospheric transmission,  $T_o$ , [Degnan, 1993] and substituted, along with the current solar and satellite zenith angles, into (1) and (5) to compute new values for the expected mean signal return and solar background. Substituting these values into the various other equations presented in this paper allows us to compute a new a priori frame interval, contrast, and frame threshold to support satellite acquisition. Once ranging data is actually being taken, the observed mean populations of the signal and noise cells can be compared to the a priori values and, if significantly different, used to further optimize the frame interval and threshold via (9) and (11). As mentioned previously, the presence of range data also allows us to correct for time bias and eliminate the slope in the data and the option to narrow the range bin and/or gate. Narrowing the gate reduces the number of range bins for a given bin width thereby reducing the frame threshold but, due to the logarithmic dependence in (11) on  $N_{bin}$ , only substantial reductions in gate width will have much of an effect. If the range bin is left unaltered, the mean fraction of signal counts falling into the signal cell will increase from  $1 - \Delta/4\tau_b$  to  $1 - \delta/4\tau_b$ . Alternatively, if the initial signal contrast is low, one can choose to reduce the bin size and increase the contrast by the ratio  $\Delta/\delta$  without affecting the mean percentage of signal counts in the cell. The increased contrast can then be exploited to reduce the frame interval and/or threshold.

Finally, it is expected that the satellite signal will be lost for brief periods of time due to intervening small clouds, pointing anomalies, mount keyhole effects, etc. causing the number of counts in the signal cell to intermittently fall below the threshold value. To recover the satellite returns obtained during these periods, a powerful second N of M test [Titterton et al, 1998; Degnan, 2002a] can be applied, if necessary, by requiring that N signal cells in M contiguous frames be *correlated*. In the most general sense, this simply means that cells tentatively identified as containing signal in adjacent frames must obey applicable physical laws or constraints. For example, the laws governing satellite motion do not allow the satellite to make unexpected discontinuous jumps into widely separated range bins between frames. Thus, we can define a *valid trajectory* as one where spacecraft position changes by no more than one range bin in moving between frames. Furthermore, the satellite must move monotonically in the correct direction on either side of the range extremum or Point of Closest Approach (PCA). For SLR, the valid trajectories are simple linear slopes as in Figure 1 except at PCA. This makes the recovery of undetected signal cells trivial via the linear interpolation between detected signal cells on opposite sides of the missing frames. In situations where an updated time bias has largely

removed the slope in the OMC plot, the signal data should fall within the same range bin for fairly long intervals (i.e. over many frames).

## REFERENCES

- Degnan, J. J., 1985, "Satellite Laser Ranging: Current Status and Future Prospects", IEEE Transactions on Geoscience and Remote Sensing, GE-23, pp. 398-413.
- Degnan, J. J., 1993, "Millimeter Accuracy Satellite Laser Ranging: A Review", Contributions of Space Geodynamics: Technology, D. E. Smith and D. L. Turcotte (Eds.), AGU Geodynamics Series, Vol. 25, pp. 133-162.
- Degnan, J. J., 2001, "Photon-counting microlaser rangers, transponders, and altimeters", Surveys in Geophysics, Vol. 22, pp.431-447.
- Degnan, J. J., 2002a, "Photon-counting multikilohertz microlaser altimeters for airborne and spaceborne topographic measurements", J. Geodynamics, Vol. 34, pp.503-549.
- Degnan, J. J., 2002b, "Asynchronous laser transponders for precise interplanetary ranging and time transfer", J. Geodynamics, Vol. 34, pp. 551-594.
- McGarry, J., Degnan, J., Titterton, P., Sweeney, H., Conklin, B., Dunn, P., 1996, "Automated tracking for advanced satellite ranging systems", Spring SPIE Meeting, Orlando Florida, April 10-11, pp. 89-102
- Titterton, P., Sweeney, H., Leonard, D., 1998, "System/Usage Impact of Operating the SLR2000 at 2 kHz", Proc. 11th International Workshop on Laser Ranging, Deggendorf, Germany, pp. 426-437, September 21-25.